Energy transfer in $Sr_{0.6}Ba_{0.4}Nb_2O_6$ through its ferroelectric phase transition

U. Caldiño
Departamento de Física, Universidad Autónoma Metropolitana-Iztapalapa,
PO Box 55-534, 09340 México, DF, México,
e-mail: cald@xanum.uam.mx

E. Martín-Rodríguez, D. Jaque and J. Garcia Solé
Departamento de Física de Materiales, Universidad Autónoma de Madrid,
Cantoblanco, 28049, Madrid, Spain,
e-mail: emma.martin@uam.es, daniel.jaque@uam.es, jose.garcia_sole@uam.es

M. Bettinelli
Dipartimento Scientifico e Tecnologico, Università di Verona, and INSTM,
UdR Verona, Strada Le Grazie 15, I-37314 Verona, Italy,
e-mail: marco.bettinelli@univr.it

Recibido el el 9 de noviembre de 2007; aceptado el 9 de agosto de 2008

Resonant $Nd^{3+} \rightarrow Yb^{3+}$ energy-transfer in the Nd^{3+} and Yb^{3+} co-doped $Sr_{0.6}Ba_{0.4}(NbO_3)_2$ (SBN) crystal is investigated by using pulsed and steady state laser spectroscopy. Spectroscopic data revealed that the energy transfer occurs via a non-radiative process. The efficiency of this energy transfer was estimated from spectral data in around 35%. Back energy transfer is not observed at the 295-415 K temperature range. A marked reduction in the luminescence intensity of Yb^{3+} ions directly excited into their $^2F_{7/2} \rightarrow ^2F_{5/2}$ transition, taking place at around 345 K, is due to the ferro to paraelectric phase transition in SBN. This thermal behavior, which is not clearly manifested when Yb^{3+} ions are excited via Nd^{3+} ions, has been explained in terms of structural changes taking place around the Yb^{3+} ions when the crystal becomes non-polar.

Keywords: Energy transfer efficiency; luminescence; spectroscopy; SBN; Nd^{3+}; Yb^{3+}; phase transition.

La transferencia de energía resonante $Nd^{3+} \rightarrow Yb^{3+}$ en el cristal $Sr_{0.6}Ba_{0.4}(NbO_3)_2$ (SBN) codopado conYb^{3+} y Nd^{3+} es investigada mediante espectroscopia láser pulsado y estacionario. Datos espectroscópicos revelaron que la transferencia de energía ocurre vía un proceso no-radiativo. La eficiencia de esta transferencia de energía fue estimada de los datos espectrales en alrededor de 35%. La transferencia de energía a la inversa ($Yb^{3+} \rightarrow Nd^{3+}$) no es observada en el rango de temperaturas 295-415 K. Una marcada reducción en la intensidad de luminiscencia de los iones Yb^{3+} directamente excitados dentro de su transición $^2F_{7/2} \rightarrow ^2F_{5/2}$, ocurriendo en alrededor de 345 K, es debida a la transición de fase ferro a paraeléctrica de SBN. Esta conducta térmica, la cual no es claramente manifestada cuando los iones Yb^{3+} son excitados vía los iones Nd^{3+}, ha sido explicada en términos de cambios estructurales ocurriendo alrededor de los iones Yb^{3+} cuando el cristal se convierte en no-polar.

Descriptores: Transferencia de energía; luminiscencia; transiciones de fase; espectroscopia; SBN; Nd^{3+}; Yb^{3+}.

PACS: 42.55.Rz; 42.62.Fi; 42.70.Hj; 42.70.Mp

1. Introduction

There is an increasing interest in nonlinear host crystals for trivalent rare earth ions, since they emerge as promising materials for tunable and pulsed coherent light generation in the visible region. So it is the case of Yb^{3+}-doped nonlinear crystals, which have interested to a great extent as potential solid-state materials emitting in the green by self-frequency doubling (SFD) of its infrared laser line (~ 1 μm) [1]. In addition, Nd^{3+}-doped non-linear crystals can be SFD and self-frequency sum mixing diode pumped solid state lasers emitting coherent radiation in the blue and green [2], because of the multiple pump channels of Nd^{3+} ion.

Strontium Barium Niobate $Sr_xBa_{1-x}Nb_2O_6$ crystal is a very interesting optical material because of its high nonlinear coefficients make this crystal as an excellent (self or external) frequency converter [2]. It is, moreover, a ferroelectric crystal with a Curie temperature (T_c) ranging from 325 to 470 K depending upon its stoichiometry ($0.25 \leq x \leq 0.75$) [3,4] or its doping [5]. Therefore, it is expected that the good properties altogether of Yb^{3+} and Nd^{3+} ions in Strontium Barium Niobate could lead to an efficient Yb^{3+} laser oscillation under Nd^{3+} pumping via energy transfer. According to all these perspectives, we have investigated the spectroscopic properties of the $Nd^{3+} \rightarrow Yb^{3+}$ energy transfer in a congruent $Sr_{0.6}Ba_{0.4}Nb_2O_6$ crystal (abbreviated SBN) as well the effect of the phase transition on the luminescence of Yb^{3+} ions sensitized by Nd^{3+} ions.

The SBN crystal has a tungsten bronze-type tetragonal structure with a P4bm space group [6]. Its general formula is $(A1)_4(A2)_2(B1)_2(B2)_8O_{30}$. The A1 sites, with C_4 symmetry, are partially occupied by Sr^{2+} ions up to 82% for $x = 0.75$ [6]. The A2 sites, with C_s symmetry, are partially occupied in a disordered way by Sr^{2+} and Ba^{2+} host cations up to 85% for $x = 0.75$ [6]. The distorted octahedral sites, B1 (C_{2v} symmetry) and B2 (C_1 symmetry),

are completely filled by Nb^{5+} cations and have sixfold coordination [6]. In SBN:Nd^{3+}:Yb^{3+} crystals Nd^{3+} ions occupy A2 sites [7], whereas that Yb^{3+} ions are located in the four different lattice sites (A1, A2, B1 and B2) [8].

2. Experimental details

Congruent SBN crystals doped with ions Nd^{3+} (0.2 at.% relative to Nb^{5+}) and/or Yb^{3+} (1 at.% relative to Nb^{5+}) were grown from fluxes consisting of mixtures of Barium and Strontium tetraborates. The concentration of Nd^{3+} and Yb^{3+} ions incorporated inside the crystal was determined by Total X-Ray Fluorescence Spectroscopy. Hereafter, the crystals studied: SBN:Nd^{3+}(0.2 at.%), SBN:Yb^{3+}(1 at.%) and SBN:Nd^{3+}(0.2 at.%):Yb^{3+}(1 at.%) will be referred as SBN:Nd, SBN:Yb and SBN:Nd:Yb, respectively.

Emission spectra were recorded by exciting with a 0.6-W fiber coupled 805 nm laser diode. The emitted light was focussed onto a SPEX 500 M monochromator, and then detected by a calibrated Germanium detector.

Luminescence decay-time measurements were made by exciting with an Optical Parametric Oscillator (OPO Quanta Ray), which provides 10-ns pulses with an average energy of 2 mJ, and then detected by means of an AsGaIn cooled photomultiplier. An EG&G lock-in amplifier was used to improve the signal to noise ratio. Decay-time data were processed by a Le Croy model LT 372 digitizing oscilloscope.

High temperature measurements were carried out by placing the crystal over a small oven platform, so that the crystal temperature could be increased at a rate of 1 K/3 min from 293 to 415 K with a stability of 0.1-0.2 K.

3. Results and discussion

a) Energy transfer $Nd^{3+} \rightarrow Yb^{3+}$.

Figure 1 shows the room temperature emission spectrum obtained in the SBN:Nd:Yb codoped crystal excited at 805 nm into the $^4I_{9/2} \rightarrow ^4F_{5/2}$ transition of Nd^{3+} ion. It consists of broad emission bands corresponding to the $Nd^{3+}(^4F_{3/2} \rightarrow ^4I_{9/2}$ and $^4F_{3/2} \rightarrow ^4I_{11/2})$ and $Yb^{3+}(^2F_{5/2} \rightarrow ^2F_{7/2})$ emissions. The Nd^{3+} emission from the $^4F_{3/2}$ metastable state involves a non-radiative decay from the $^4F_{5/2}$ state. Considering that Yb^{3+} ions cannot be excited at 805 nm (see Yb^{3+} absorption spectrum in Fig. 2), then the Yb^{3+} emission is produced through the Nd^{3+} excitation by means of energy transfer. A schematic diagram of energy positions for the different $^{2S+1}L_J$ states of Nd^{3+} and Yb^{3+} ions in SBN [9] is portrayed in the inset of Fig. 1 for the sake of clarity.

The Nd^{3+} to Yb^{3+} ion energy transfer is expected to occur in SBN:Nd:Yb since the Nd^{3+} $(^4F_{3/2} \rightarrow ^4I_{9/2})$ emission overlaps the $Yb^{3+}(^2F_{7/2} \rightarrow ^2F_{5/2})$ absorption [10] as can be appreciated in Fig. 2.

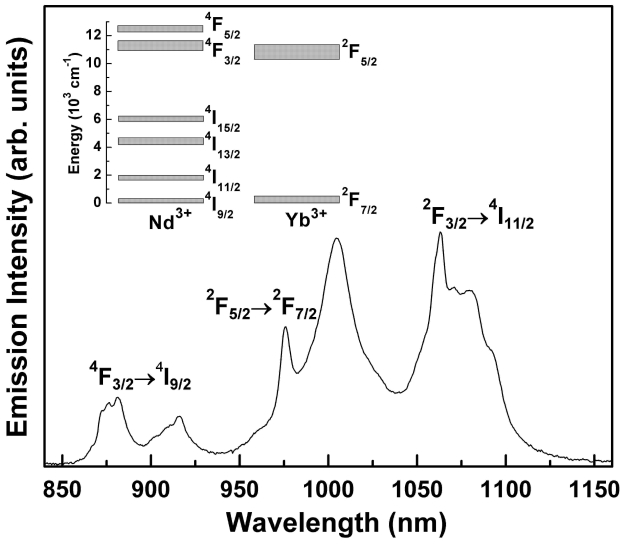

FIGURE 1. Emission spectrum of SBN:Nd:Yb excited at 805 nm. The inset displays an energy level diagram of $Nd^{3+}$and Yb^{3+} ions in SBN [9].

The $^4F_{3/2} \rightarrow ^4I_{9/2}$ emission displayed in this figure was recorded from the SBN:Nd singly doped crystal excited at 805 nm. The spectral overlap between the sensitizer emission and acceptor absorption is a necessary condition for the occurrence of the energy transfer. Consequently, the presence of $Nd^{3+} \leftarrow Yb^{3+}$ back energy transfer by means of $Yb^{3+}(^2F_{5/2})$, $Nd^{3+}(^4I_{9/2}) \rightarrow Yb(^2F_{7/2})$, $Nd(^4F_{3/2})$ cross relaxation can be unable due to the vanishing overlap between the Yb^{3+} emission and Nd^{3+} absorption [11], as shown in the inset of Fig. 2. The Yb^{3+} $(^2F_{5/2} \rightarrow ^2F_{7/2})$ emission displayed in the inset of Fig. 2 was obtained form the SBN:Yb singly doped crystal excited at 903 nm.

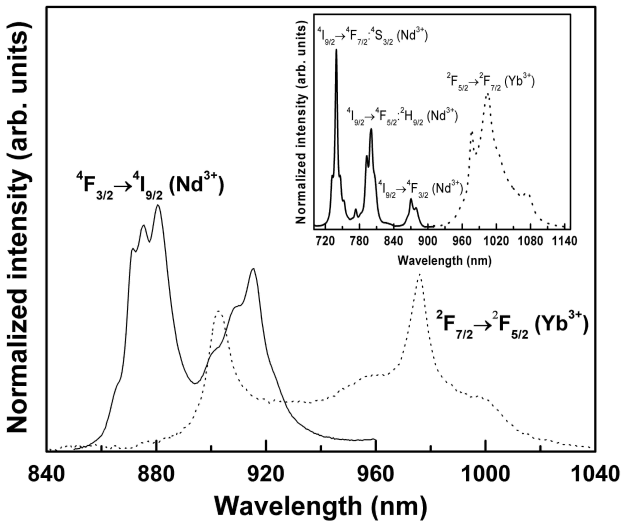

FIGURE 2. Overlap region between the Nd^{3+} emission (solid line) and the Yb^{3+} absorption [10] (dashed line) in SBN. The inset shows spectra of Nd^{3+} absorption [11] (solid line) and Yb^{3+} emission (dashed line) in SBN.

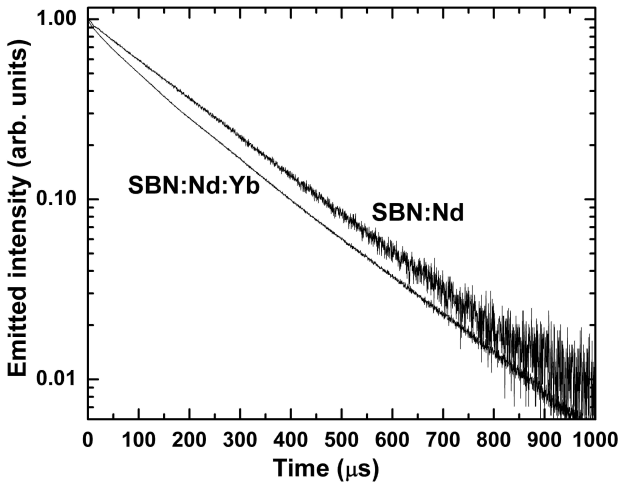

FIGURE 3. Time evolution of the Nd^{3+} emission ($^4F_{3/2} \rightarrow {}^4I_{11/2}$) obtained for the crystals SBN:Nd and SBN:Nd:Yb excited at 870 nm.

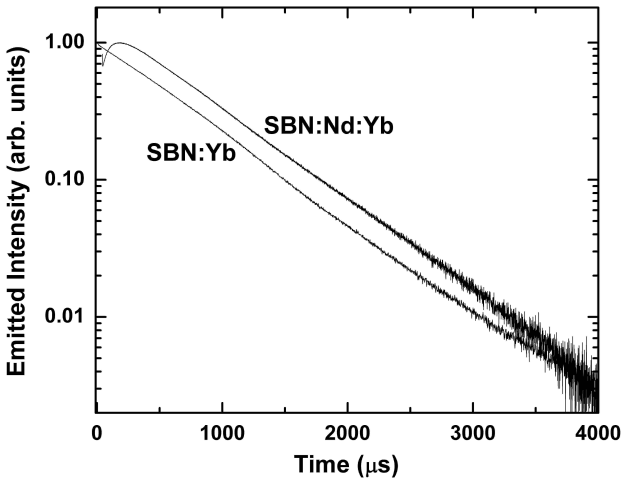

FIGURE 4. Time evolution of Yb^{3+} emission (1004 nm) obtained for the SBN:Nd:Yb and SBN:Yb crystals excited at 870 and 903 nm, respectively.

Figure 3 shows the room temperature Nd^{3+} ($^4F_{3/2} \rightarrow {}^4I_{11/2}$) emission intensity (monitored at 1060 nm) versus decay-time for the SBN:Nd and SBN:Nd:Yb crystals excited at 870 nm into the $^4I_{9/2} \rightarrow {}^4F_{3/2}$ transition of Nd^{3+}. It can be observed that by co-doping the SBN:Nd crystal with Yb^{3+} ions an increase is observed in the decay rate of the Nd^{3+} ion emission. This fact indicates that $Nd^{3+} \rightarrow Yb^{3+}$ energy transfer is taking place via a non-radiative process.

b) Back energy transfer $Nd^{3+} \leftarrow Yb^{3+}$

The possibility of $Nd^{3+} \leftarrow Yb^{3+}$ back energy transfer in SBN:Nd:Yb has been investigated by analyzing

(i) the decay-time of Yb^{3+} luminescence for the (SBN:Yb) singly doped and (SBN:Nd:Yb) codoped crystals and

(ii) the emission spectrum obtained under Yb^{3+} excitation for the codoped crystal:

(i) The time dependence of the Yb^{3+} emission, obtained under Nd^{3+} excitation at 870 nm, exhibits an excitation rise at a rate in accordance with excitation via energy transfer from Nd^{3+} ions. After this initial rise, related to the $^4F_{3/2}$ state (Nd^{3+}) fluorescence lifetime, the Yb^{3+} luminescence presents an exponential decay-time. Figure 4 shows room temperature Yb^{3+} luminescence decay-time curves (monitored at 1004 nm) obtained for the SBN:Nd:Yb and SBN:Yb crystals exciting Nd^{3+} ions up to their $^4F_{3/2}$ state (870 nm) and Yb^{3+} ions up to their $^2F_{5/2}$ state (903 nm), respectively. In the crystal codoped the decay-time curve shows a rise time of about 160 μs, followed by an exponential decay with a lifetime of about 625 μs, essentially the value obtained for the SBN:Yb singly doped crystal excited at 903 nm.

(ii) The emission spectrum obtained in the codoped crystal under Yb^{3+} ion excitation (at 903 nm) shows only the broad emission band characteristic of Yb^{3+} ions without any contribution from Nd^{3+} ions even at high temperature (415 K) as can be appreciated from Fig. 5.

From these two results, (i) and (ii), it can be inferred that back transfer from Yb^{3+} to Nd^{3+} ions is not important. As expected, the absence of this back transfer must be a consequence of a vanishing overlap between the Yb^{3+} emission and Nd^{3+} absorption, as shown in the inset of Fig. 2. Taking into account that $Nd^{3+} \leftarrow Yb^{3+}$ back transfer can be considered negligible in comparison to the $Nd^{3+} \rightarrow Yb^{3+}$ direct energy transfer, then the $Nd^{3+} \rightarrow Yb^{3+}$ energy transfer efficiency η_t can be estimated from the emission spectrum displayed in Fig. 1 using the following equation [9]:

$$\eta_t \approx \frac{\frac{1}{\eta_{Yb}} \int_{850\,\mathrm{nm}}^{1150\,\mathrm{nm}} I_{Yb}(\lambda)d\lambda}{\left(1 + \frac{\beta_{4_{I_{13/2}}} + \beta_{4_{I_{15/2}}}}{\beta_{4_{I_{9/2}}} + \beta_{4_{I_{11/2}}}}\right) \frac{1}{\eta_{Nd}} \int_{850\,\mathrm{nm}}^{1150\,\mathrm{nm}} I_{Nd}(\lambda)d\lambda + \frac{1}{\eta_{Yb}} \int_{850\,\mathrm{nm}}^{1150\,\mathrm{nm}} I_{Yb}(\lambda)d\lambda}. \quad (1)$$

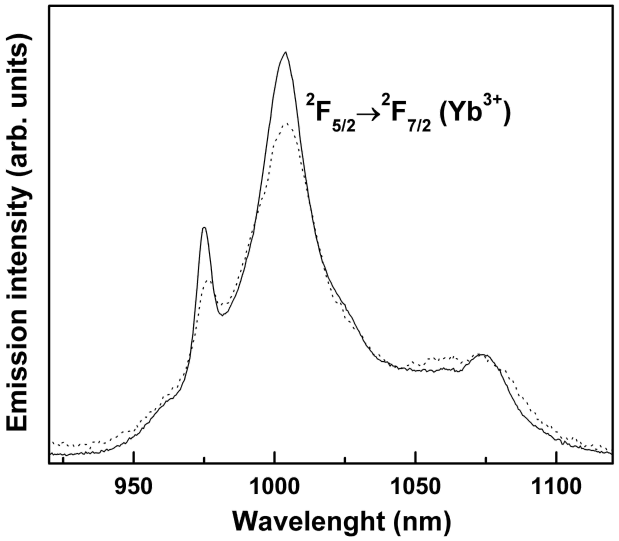

FIGURE 5. Emission spectra of SBN:Nd:Yb excited at 903 nm at room temperature (solid line) and 415 K (dashed line). The spectra have been normalized to the lower energy emission band peaking at 1074 nm.

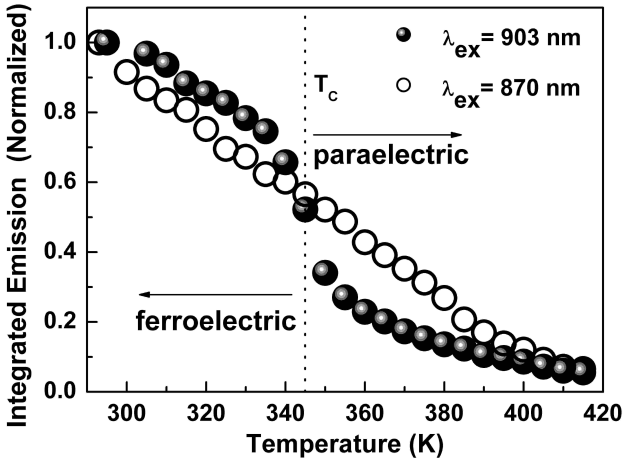

FIGURE 6. Temperature dependence of the Yb^{3+} emission intensity after excitation of the $Yb^{3+}{}^2F_{5/2}$ level at 903 nm and Nd^{3+} $^4F_{3/2}$ level at 870 nm.

So that a net transfer efficiency of about 35 % is obtained after using the branching ratios previously reported for the Nd^{3+} in SBN ($\beta_{^4I_{9/2}} = 0.396$, $\beta_{^4I_{11/2}} = 0.5$, $\beta_{^4I_{13/2}} = 0.1$ and $\beta_{^4I_{15/2}} = 0.004$ [11]), and the intrinsic fluorescence quantum efficiencies of both Nd^{3+} ($\eta_{Nd} \approx 0.8$ [9]) and Yb^{3+} ($\eta_{Yb} \approx 0.9$ [9]).

(c) Luminescence of SBN:Nd:Yb along phase transition

In order to investigate the effect of the phase transition on the luminescence of Yb^{3+} ions in the SBN:Nd:Yb crystal, the spectral evolution of their $^2F_{5/2} \rightarrow {}^2F_{7/2}$ emission, exciting at 870 nm ($^4F_{3/2}$ state of Nd^{3+}) and 903 nm ($^2F_{5/2}$ state of Yb^{3+}), has been systematically investigated as a function of temperature from 293 to 415 K. Each emission spectrum was recorded after a sufficient time to ensure that a steady state temperature was achieved. Figure 6 displays the variation of the Yb^{3+} emitted intensity (measured as the area under the emission spectrum) as a function of crystal temperature after 870 and 903 nm excitation. The Yb^{3+} overall luminescence is reduced with temperature increasing. It can also be noticed a marked reduction in the luminescence intensity of Yb^{3+} ions taking place at around 345 K, when these ions are excited at 903 nm. The marked intensity decrease of the Yb^{3+} emission can be attributed to the presence of the ferro to paraelectric phase transition. This thermal behavior of the Yb^{3+} luminescence, which is not clearly manifested when Yb^{3+} ions are excited via Nd^{3+} ions, at 870 nm, has been explained invoking the sites occupied by Yb^{3+} ions in the ferroelectric (polar) phase and how the local structure of such sites is modified in the paraelectric (non polar) phase. In the polar phase the Yb^{3+} ions occupying the A_1, A_2, B_1 and B_2 cationic lattice sites have C_4, C_s, C_{2v} and C_1 local symmetries, respectively [8,12]. According to one of the models used to describe the non polar phase [6], the A_1, A_2 and B_1 sites adopt C_{4h}, C_{2v} and D_{2h} symmetries, respectively, while the B_2 site remains in its C_1 original symmetry. Taking into account that the C_{4h} and D_{2h} groups have inversion symmetry, then the Yb^{3+} ions located in the A_1 and B_1 sites produce very weak emissions (magnetic dipole allowed transitions) in the paraelectric phase. The quenching of the luminescence of $Yb^{3+}(A_1)$ and $Yb^{3+}(B_1)$ ions in the paraelectric phase induces a strong decrease in the Yb^{3+} luminescence above T_c. Thus, the luminescence remaining in the non polar phase can be attributed to the $Yb^{3+}(A_2)$ and $Yb^{3+}(B_2)$ ions [8,12]. Therefore, the room temperature luminescence of Yb^{3+} ions in SBN:Nd:Yb (after Yb^{3+} excitation at 903 nm) is produced by these ions located in the four different lattice sites (A1, B1, A2, B2).

In the paraelectric phase those Yb^{3+} ions located in the A1 and B1 sites, which are occupying centrosymmetric positions, become dead sites, so that their emission is quenched [8,12]. On the other, the luminescence of Yb^{3+} ions excited via Nd^{3+} ions (at 870 nm) dose not show such abrupt intensity decrease of the Yb^{3+} emission in the ferro to paraelectric phase transition. This fact suggests that the occupancy of Yb^{3+} ions sensitized by Nd^{3+} ions could be predominantly restricted to a less number of sites in SBN (A2 and B2), and so their luminescence is weakly sensitive to temperature changes around phase transition. Anyway, it would be necessary to explore the possibility of following the ferroelectric phase transition through fluorescence spectroscopy under high pressure at low temperature in the SBN:Nd:Yb crystal, since this spectroscopic technique allows for the analysis of the local structure of the different cationic sites of Yb^{3+} both in the ferroelectric and paraelectric phases [12].

4. Conclusions

Resonant $Nd^{3+} \rightarrow Yb^{3+}$ energy-transfer takes place in the Nd^{3+} and Yb^{3+} ion co-doped $Sr_{0.6}Ba_{0.4}(NbO_3)_2$ (SBN) crystal as a consequence of a significant spectral overlap. The $Nd^{3+} \rightarrow Yb^{3+}$ energy transfer occurs via a non-radiative process. The efficiency of this energy transfer was estimated from spectral data and resulted in being about 35 %. Back energy transfer is not observed at the 295-415 K temperature range. The ferro to paraelectric phase transition (at around 345 K) is clearly manifested in the SBN:Nd:Yb codoped crystal through a marked reduction in the Yb^{3+} luminescence intensity under direct excitation of the Yb^{3+} ions at temperature around 345 K. However, such phase transition is not clearly observed when Yb^{3+} ions are excited via Nd^{3+} ions. Therefore, the sensitivity of the Yb^{3+} ion luminescence to the ferro to paraelectric phase transition in the SBN:Nd:Yb crystal is strongly related to the distribution of Yb^{3+} ions among the four available cationic sites: A_1, A_2, B_1 and B_2. Ytterbium ions excited up to their $^2F_{5/2}$ state are distributed among these four sites, so that their luminescence features are very sensitive to phase transition. This is not the case of Yb^{3+} ions sensitized by Nd^{3+} ions, whose occupancy could be restricted to a less number of sites in SBN, and so their luminescence is weakly sensitive to temperature changes around phase transition.

Acknowledgments

This work has been supported by the Spanish Ministry of Science and Technology under project contract MAT2004-03347 and by the CONACyT (México) under project contract 43016-F.

1. E. Montoya, J. Capmany, L.E. Bausá, T. Kellner, A. Diening, and G. Huber, *Appl. Phys. Lett.* **74** (1999) 3113.
2. J.J. Romero, D. Jaque, J. García-Solé, and A.A. Kaminskii, *Appl. Phys. Lett.* **78** (2001) 1961.
3. C. David, *et al.*,*Phys. Stat. Sol. (a)* **201** (2004) R49.
4. A. Speghini, *et al., J. Phys. D: Appl. Phys.* **39** (2006) 4930.
5. T. Volket *et al., Phys. Solid State* **42** (2000) 2129.
6. P.B. Jamieson, S.C. Abrahams, and J.L. Bernstein, *J. Chem. Phys.* **48** (1968) 5048.
7. M.O. Ramírez, D. Jaque, L.E. Bausá, J. García-Solé and A.A. Kaminskii, *Phys. Rev. Lett.* **95** (2005) 267401.
8. M.O. Ramírez, *et al.*, *Phys. Rev.* B **73** (2006) 035119.
9. U. Caldiño, *et al. Physical Review* B **77** (2008) 75121.
10. M.O. Ramírez, D. Jaque, L. Ivleva, and L.E. Bausá, *J. Appl. Phys.* **95** (2004) 6185.
11. J.J. Romero, *Ph. Thesis* (2002) unpublished.
12. M.O. Ramírez, L.E. Bausá, J. García Solé, A. Kaminska, S. Kobyakov and A. Suchocki, *Phys. Rev.* B **74** (2006) 174113.